Crystal Structure and Functional Characterization of Yeast YLR011wp, an Enzyme with NAD(P)H-FMN and Ferric Iron Reductase Activities

Dominique Liger, Marc Graille, Cong-Zhao Zhou, Nicolas Leulliot, Sophie Quevillon-Cheruel, Karine Blondeau, Joël Janin, Herman van Tilbeurgh

THE JOURNAL OF BIOLOGICAL CHEMISTRY
Vol. 279, No. 33, Issue of August 13, pp. 34890–34897, 2004

Printed in U.S.A.

Crystal Structure and Functional Characterization of Yeast YLR011wp, an Enzyme with NAD(P)H-FMN and Ferric Iron Reductase Activities*

Received for publication, May 14, 2004, and in revised form, June 3, 2004
Published, JBC Papers in Press, June 7, 2004, DOI 10.1074/jbc.M405404200

Dominique Liger‡§, Marc Graille¶§, Cong-Zhao Zhou‡‖, Nicolas Leulliot‡, Sophie Quevillon-Cheruel‡, Karine Blondeau, Joël Janin¶, and Herman van Tilbeurgh‡¶‡‡**

*From the ‡Institut de Biochimie et de Biophysique Moléculaire et Cellulaire (CNRS-Unité Mixte de Recherche (UMR) 8619), Université Paris-Sud, Bâtiment 430, 91405 Orsay, France, ¶Laboratoire d'Enzymologie et Biochimie Structurales (CNRS-Unité Propre de Recherche 9063), Bâtiment 34, 1 Avenue de la Terrasse, 91198 Gif sur Yvette, France, and **Institut de Génétique et Microbiologie (CNRS-UMR 8621), Université Paris-Sud, Bâtiment 360, 91405 Orsay, France*

Flavodoxins are involved in a variety of electron transfer reactions that are essential for life. Although FMN-binding proteins are well characterized in prokaryotic organisms, information is scarce for eukaryotic flavodoxins. We describe the 2.0-Å resolution crystal structure of the *Saccharomyces cerevisiae YLR011w* gene product, a predicted flavoprotein. YLR011wp indeed adopts a flavodoxin fold, binds the FMN cofactor, and self-associates as a homodimer. Despite the absence of the flavodoxin key fingerprint motif involved in FMN binding, YLR011wp binds this cofactor in a manner very analogous to classical flavodoxins. YLR011wp closest structural homologue is the homodimeric *Bacillus subtilis* Yhda protein (25% sequence identity) whose homodimer perfectly superimposes onto the YLR011wp one. Yhda, whose function is not documented, has 53% sequence identity with the *Bacillus* sp. OY1–2 azoreductase. We show that YLR011wp has an NAD(P)H-dependent FMN reductase and a strong ferricyanide reductase activity. We further demonstrate a weak but specific reductive activity on azo dyes and nitrocompounds.

The most frequently used cofactors in enzymatic redox reactions are the pyridine (NAD and NADP) and the flavin (FAD and FMN) nucleotides. Although NAD and NADP are soluble cofactors used by dehydrogenases, FAD and FMN usually work as prosthetic groups in flavoproteins to which they are tightly bound. Flavodoxins are small monomeric flavoproteins (15–22 kDa) that noncovalently bind a single FMN molecule, acting as a redox center (1). The flavodoxin scaffold contributes to the mechanism of electron transfer by stabilizing the FMN molecule in an environment that promotes the highly negative redox potential required for its biochemical activity. This is accomplished by sandwiching the FMN ring between two hydrophobic side chains. Flavodoxins are involved in a variety of electron transfer reactions that are essential in the metabolism of pyruvate (2), nitrogen, and pyridine nucleotides (3). These enzymes exist under three redox states: oxidized; partially reduced (semiquinone); and fully reduced (hydroquinone). Until now, flavodoxins have been identified in many prokaryotes and also in some eukaryotic algae (4–6). In mammalian systems, flavodoxins have only been found as domains inserted in larger redox proteins such as cytochrome P450 reductase where they act as the electron transport intermediate between FAD and the P450 iron center (7). Flavodoxin-like domains are also found in mammalian nitric-oxide synthase (8) and in human erythrocyte NADPH-flavin reductase (9).

The *Saccharomyces cerevisiae YLR011w* open reading frame codes for a protein of unknown function that has been found to be up-regulated in response to low temperature exposure (10). The sequence belongs to a COG4530 (Cluster of Orthologous Genes) predicted to generally contain flavoproteins. Hence, the YLR011wp 21-kDa protein was proposed to be composed of a single domain present in NADPH-dependent FMN reductases. We have solved the 2-Å resolution crystal structure, confirming that it adopts a flavodoxin fold and binds the FMN cofactor. YLR011wp exists as a dimer in the crystal as well as in solution. The YLR011wp closest structural homologue is the *Bacillus subtilis* Yhda protein (Protein Data Bank code 1NNI) (11), whose function is not documented but has 53% sequence identity with the *Bacillus* sp. OY1–2 azoreductase. These enzymes are responsible for the reductive cleavage of azo dyes. Organisms producing azoreductase present a biotechnological interest for the early step in detoxification of industrial dyes. This type of activity has not been reported before in *S. cerevisiae*. Therefore, we have attempted to characterize YLR011wp reductase activity by testing different azo dyes and nitrocompounds but also ferricyanide as electron acceptors.

EXPERIMENTAL PROCEDURES

Cloning and Purification—The *YLR011w* open reading frame DNA was amplified by PCR using oligodeoxynucleotides synthesized by MWG Biotech and cloned between the NdeI and NotI sites of pET29 vector from Novagen. The expression strain Rosetta was obtained from Novagen. 2× YT medium (5 g of NaCl, 16 g of Bactotryptone; 10 g of yeast extract) was purchased from BIO 101, Inc., and isopropyl-β-D-thiogalactopyranoside was purchased from Sigma. Transformed Rosetta cells were grown at 37 °C up to an $A_{600\ nm}$ of 1. Expression was induced with 0.5 mM isopropyl-β-D-thiogalactopyranoside, and the cells were grown for a further 12 h at 15 °C. Cells were collected by centrifugation, washed, and resuspended in lysis buffer (20 mM Tris-HCl, pH 8, 300 mM NaCl, 10 mM β-mercaptoethanol) at 4 °C. Cells were lysed by 3 cycles of freeze-thawing and 30 s of sonication and then were centrifuged. The His-tagged proteins were purified using a Ni^{2+} affinity

* This work is supported in part by grants from the Ministère de la Recherche et de la Technologie (Programme Génopoles) and the Association pour la Recherche sur le Cancer (to M. G.). The costs of publication of this article were defrayed in part by the payment of page charges. This article must therefore be hereby marked "*advertisement*" in accordance with 18 U.S.C. Section 1734 solely to indicate this fact.

The atomic coordinates and structure factors (code 1T0I) have been deposited in the Protein Data Bank, Research Collaboratory for Structural Bioinformatics, Rutgers University, New Brunswick, NJ (http://www.rcsb.org/).

§ Both authors contributed equally to the work.

‖ Present address: School of Life Science, University of Science and Technology of China, Hefei Anhui 230027, People's Republic of China.

‡‡ To whom correspondence should be addressed. Tel.: 33-1-69-82-34-91; Fax: 33-1-69-82-31-29; E-mail: herman@lebs.cnrs-gif.fr.

column (Qiagen Inc.) according to the standard protocols. Eluted protein was further purified by gel filtration using a Superdex™ 75 column (Amersham Biosciences) equilibrated against the buffer containing 20 mM Tris-HCl, pH 8, 100 mM NaCl, and 20 mM β-mercaptoethanol. The purity of the pooled fractions was checked by SDS-PAGE, and the integrity of the protein samples was checked by mass spectrometry. Selenium Met (Se-Met)[1]-labeled proteins were prepared as follows. Transformed cells were grown in M63 medium at 37 °C up to an $A_{600\ nm}$ of 1. The culture then was complemented with a mixture of amino acids (L-Lys, L-Phe, and L-Thr at 100 mg/liter and L-Ile, L-Leu, L-Val, and L-Se-Met at 50 mg/liter) within 30 min, and the recombinant protein was overexpressed by the addition of 0.3 mM isopropyl-β-D-thiogalactopyranoside within 12 h at 15 °C. The protein was purified as described above. Seleno-methionine incorporation into the protein was >95% as assayed by mass spectrometry.

Crystallization and Resolution of the Structure—Native and Se-Met labeled protein samples were stored in 20 mM Tris-HCl, pH 8, 100 mM NaCl, and 20 mM β-mercaptoethanol. Prior to crystallization screenings, 20 mM $CaCl_2$ and 2 mM FMN were added to the protein solutions. Crystals of both the native and Se-Met-labeled protein were grown from a 1:1-μl mixture of protein (6 mg/ml) with 10–15% polyethylene glycol 3000, 20% polyethylene glycol 400, and 0.1 M Tris-HCl, pH 8.5 (reservoir solution). Crystals with a maximal size of 100–200 μm appeared within 3 days. For data collection, the crystals were frozen in liquid nitrogen after soaking in cryoprotectant buffer containing 10% polyethylene glycol 3000, 30% polyethylene glycol 400, and 0.1 M Tris-HCl, pH 8.5. Crystals of the native and Se-Met labeled proteins diffracted to 1.9 and 2.3 Å, respectively (beamline BM30A at the European Synchrotron Radiation Facility, Grenoble, France) (12).

The structure was determined using single wavelength anomalous dispersion x-ray diffraction data collected from the Se-Met derivative crystal. Data were processed using the HKL package (13). The space group was $P2_12_12$ with two molecules per asymmetric unit. Two selenium atom sites of three were found for each monomer with the program SOLVE in the 80–2.8-Å resolution range (14). After solvent flattening and phase extension to a 2.3-Å resolution with the program RESOLVE (15), the quality of the electron density map allowed the manual construction of most of the secondary structure elements with the TURBO molecular modeling program (16). The model was completed using iterative cycles of model building using TURBO and refinement with the REFMAC program (17). The final model contains residues 1–185 from monomer A, residues 2–30 and 39–186 from monomer B, two FMN molecules, two calcium ions, and 111 water molecules. All of these residues have well defined electron density and fall within the allowed regions of the Ramachandran plot as defined by the program PROCHECK (18). Data collection and refinement statistics of the structure are summarized in Table I.

Enzyme Assays—YLR011wp was assayed for FMN reductase activity in a reaction mixture (1 ml of final volume) consisting of 150 μM NADH or NADPH, 100 μM FMN, and 0.24 μM enzyme in 25 mM Tris-HCl, pH 7.5. NAD(P)H oxidization was followed at 30 °C by measuring the decrease in absorbance at 340 nm (ϵ_M = 6.22 mM^{-1} cm^{-1}).

Azoreductase assay was performed in a reaction mixture (1 ml) containing 35 μM azo dye, 100 μM NADH or NADPH, 20 μM FMN, and 2.4 μM of enzyme in 25 mM Tris-HCl, pH 7.5. The reaction was run at 30 °C, and the initial rate was determined by monitoring the decrease in absorbance at optimal wavelength for each azo dye tested as a substrate: 430 nm for Methyl Red (4-(dimethylamino)azobenzene-2′-carboxylic acid); 450 nm for Ethyl Red (4-(diethylamino)azobenzene-2′-carboxylic acid); 485 nm for Orange II (4-(2-hydroxy-1-naphthylazo)-benzenesulfonic acid); and 597 nm for Reactive Black 5.

NAD(P)H-ferricyanide reductase assay was performed in a reaction mixture (1 ml) consisting of 150 μM NADH or NADPH, 100 μM ferricyanide (potassium hexacyanoferrate(III), $K_3Fe(CN)_6$) and 9 nM of enzyme in 25 mM Tris-HCl, pH 7.5. Ferricyanide reduction was followed at 30 °C by measuring the decrease in absorbance at 420 nm (ϵ_M = 1 mM^{-1} cm^{-1}). The effect of FMN on YFL011wp NAD(P)H-ferricyanide reductase activity was tested by the addition of 20 μM FMN to the reaction mixture.

YLR011wp was also assayed for nitroreductase activity. The reaction mixture and protocol were identical as for the ferricyanide reductase assay with the exception that ferricyanide was replaced by nitrofurazone and activity was monitored by measuring the decrease in absorbance at 400 nm (ϵ_M = 12.96 mM^{-1} cm^{-1}).

[1] The abbreviations used are: Se-Met, selenium Met; r.m.s.d., root mean square deviation.

RESULTS AND DISCUSSION

Overall Structure—The crystal structure of the 21-kDa YLR011w protein was solved by single wavelength anomalous dispersion phasing using Se-Met-substituted protein crystals. The asymmetric unit of the crystal contains two YLR011wp molecules with identical structures (the r.m.s.d. for 229 Cα positions is 0.44 Å). Refinement of the structure against 2-Å resolution native data yielded R and R_{free} factors of 20.4 and 26%, respectively. All of the residues of the final model are well defined in the $2F_o - F_c$ electron density map and occupy favorable regions of the Ramachandran plot as defined by PROCHECK (18). All of the refinement data are gathered in Table I.

The YLR011wp monomer is a globular α/β protein of approximate dimensions of 50 × 30 × 30 $Å^3$. The structure of the YLR011wp has a single domain flavodoxin-like architecture with a central five-stranded parallel β-sheet (strand order β2, β1, β3, β4, and β5) flanked by helices α1 and α5 on one side and by three helices (α2–α4) on the other side (Fig. 1*a*). Searches for the closest structural analogues of YLR011wp using the EBI Macromolecular structure data base (www.ebi.ac.uk/msd/) revealed good matches (Z score values between 6.5 and 6. 9) with many flavodoxin proteins such as *B. subtilis* Yhda protein (25% sequence identity, r.m.s.d. of 1.8 Å over 143 Cα positions) (Protein Data Bank code 1NNI) and flavodoxins from the cyanobacterium *Anabaena* (14% sequence identity, r.m.s.d. of 1.9 Å over 118 Cα positions) (19) and from *Helicobacter pylori* (17% sequence identity, r.m.s.d. of 1.9 Å over 117 Cα positions) (6).

Flavodoxins have been classified into two subfamilies: 1) short-chain flavodoxins, which are roughly 150 residues long, and 2) long-chain flavodoxins with an insertion of ~20 amino acid residues in the middle of the last strand of the β-sheet (20). Although YLR011wp is made up of 191 residues, its final β-strand (β5 in Fig. 1*a*) has no insert and hence this protein belongs to the short-chain flavodoxin subfamily. The extra 40 amino acid residues of YLR011wp are part of two other insertions relative to classical short-chain flavodoxins. The first insertion (Leu^{45}-Leu^{85}) is found in the segment connecting strands β2 and β3 and containing helix α2. This region is longer by 30 amino acids compared with classical flavodoxins. The N-terminal part of this segment is involved in homodimer formation (see below). The second 10-residue insertion (Pro^{156}-Ile^{166}) is found in the linker between strand β5 and the C-terminal helix α5. These two insertions are located at each extremity of the YLR011wp monomer. Because of the head-to-tail organization of the homodimer (see below), the first insertion from monomer A is facing the second insertion from monomer B (Fig. 2*a*). This dimer contact forms a closed lid that completely hides the dimethyl benzene part of the isoalloxazine moiety of the FMN molecule (see below).

FMN Binding—Because YLR011wp sequence analysis suggests that it is entirely made up by a FMN binding domain as found in the NADPH-dependent FMN reductases, we incubated the protein with 2 mM FMN prior to the initial crystallization screening. During refinement of the structure, inspection of the electron density maps clearly revealed the presence of a bound FMN cofactor in each monomer. As observed for other flavodoxins, the cofactor lies on top of the C-terminal end of the YLR011wp central β-sheet inside a positively charged pocket (Fig. 1*a*). The FMN phosphoribityl moiety is deeply buried in the protein, whereas the isoalloxazine ring remains partially accessible to the solvent. Each FMN is in contact with both monomers, and only 10% of its surface is solvent-accessible. The main contribution of YLR011wp to FMN binding comes from three loops. The linker that is connecting strand β1 to helix α1 is in contact with the phosphoribityl moiety,

TABLE I
Data collection and refinement statistics
Values in parentheses are for highest resolution shell. SAD, single wavelength anomalous dispersion.

	Native	SAD
Data collection		
Resolution (Å)	35–1.90 (1.94–1.90)	80–2.30 (2.35–2.30)
Space group	$P2_12_12$	$P2_12_12$
Unit cell parameters (Å)	a = 62.9; b = 110.2; c = 50.1	a = 63; b = 110.2; c = 50.4
Total number of reflections	118,038	189,586
Total number of unique reflections	27,164	28,656
R_{sym} (%)[a]	6.3 (53.7)	6.1 (44.3)
Completeness (%)	96.9 (95.5)	95.1 (94.3)
$I/\sigma(I)$	21.8 (1.7)	25.3 (2.5)
Redundancy	4.3	6.6
Phasing		
Resolution (Å)		80–2.80
Figure of merit (after density modification)		0.285 (0.54)
Refinement		
Resolution (Å)	10–2.0	
R/R_{free} (%)[b]	19.9/25.4	
R.m.s.d. bonds (Å)	0.003	
R.m.s.d. angles (°)	0.743	
Mean B factor (Å^2)		
Protein/FMN/	43/29	
Calcium/water	30/40	
Ramachandran plot (%)		
Most favored	94.9	
Allowed	5.1	

[a] $R_{merge} = \Sigma_h\Sigma_i|I_{h,i} - \langle I_h\rangle|/\Sigma_h\Sigma_iI_{h,i}$, where $I_{h,i}$ is the ith observation of the reflection h, whereas $\langle I_h\rangle$ is the mean intensity of reflection h.
[b] $R_{factor} = \Sigma||F_o| - |F_c||/|F_o|$. R_{free} was calculated with a small fraction (5%) of randomly selected reflections.

whereas the loops between strand β3 and helix α3 and between strand β4 and helix α4 are interacting with both FMN parts. In total, each FMN molecule forms 12 direct hydrogen bonds (Table II) and shields 570 Å^2 of its surface from the solvent upon complex formation with the homodimer.

The isoalloxazine ring is mainly in contact with residues from the loops connecting strand β3 to helix α3 (Pro^{93}-Trp^{97}) and strand β4 to helix α4 (Gly^{125}-Gly^{129}), completed by contacts with Ile^{60} and Asp^{108} from the other monomer. It is stabilized by five direct hydrogen bonds with the protein and has three water molecules bound. The pyrimidine end of the isoalloxazine is hydrogen-bonded to the Gln^{94} side chain (N_3 atom from FMN) and to three main chain amide groups (Asn^{96} H-bonds to FMN N_5 and O_4 atoms, whereas Trp^{97} and Gly^{126} H-bond to FMN O_4 and O_2 atoms, respectively). The *re*-face of the isoalloxazine ring lies against the hydrophobic side chain from Tyr^{95}, whereas its partly solvent-exposed *si*-face is in contact with Ile^{60} from the neighbor monomer.

The phosphoribityl moiety of the molecule is mainly stabilized by electrostatic interactions (Fig. 1*b*). The ribitol part of the FMN molecule directly interacts with Arg^{11}, Val^{15}, Pro^{93}, Tyr^{124}, Gly^{125}, and Val^{157}. Two oxygen atoms (O_2* and O_4*) from this FMN moiety are indirectly hydrogen-bonded to the protein backbone by water molecules. The FMN O_4* atom is hydrogen-bonded to three residues from the second insertion region, *i.e.* the loop connecting strand β5 to helix α5 (Gly^{58} amide and Pro^{156} and Thr^{159} carbonyls), whereas its O_2* atom forms H-bonds with Gln^{94} amide and Tyr^{124} carbonyl groups.

The FMN phosphate group forms a bidentate salt bridge with Arg^{11} and five hydrogen bonds (Fig. 1, *b* and *c*, and Table II) with the Ser^9, Tyr^{95}, and Tyr^{124} hydroxyl groups as well as with the Val^{15} and Cys^{16} amides from the β1–α1 loop. This latter loop is the most invariant feature of the flavodoxin fold. It bears the flavodoxin key fingerprint motif ((T/S)*X*TG*X*T), which is always involved in interaction with the FMN phosphate moiety (5). Interestingly, the *S. cerevisiae* YLR011wp FMN phosphate binding loop sequence (SVRAKRVC) (Fig. 3) does not match the flavodoxin signature and is longer by 2 residues. This results in a clearly different conformation from that of the canonical loop (r.m.s.d of the Cα atoms of the key fingerprint motif around 3 Å between YLR011wp and flavodoxins), whereas this region varies by <1 Å within the more classical flavodoxins. Despite these differences, the YLR011wp FMN phosphate binding pocket is reminiscent of the corresponding pocket in the typical flavodoxin proteins (Table II). In flaxodoxins, the FMN phosphate oxygens are in interaction with the amide groups of the five residues (*X*TG*X*T) from the loop motif as well as with the Oγ1 and Nε1 atoms of Thr^{14} and Trp^{57}, two invariant residues in bacterial flavodoxins (Fig. 1*d*). In YLR011wp, only two hydrogen bonds are made with the amide groups (Val^{15} and Cys^{16} in place of Val^{13} and Thr^{14}) but Arg^{11} Nε and Nη1 atoms replace the amide groups from residues at positions 10 and 11 (Gln and Thr in the case of *Anacystis nidulans*) (5) (Table II and Fig. 1, *c* and *d*). Similarly, residues Thr^{14} and Trp^{57}, which are invariant in classical flavodoxins but not conserved in YLR011wp (Fig. 3), are substituted by Tyr^{124} and Tyr^{95} (this Tyr^{95} is invariant in YLR011wp orthologues) hydroxyl groups as hydrogen bond donor.

The vast majority of flavodoxin domains whose structure is known have the six-residue-long flavodoxin key fingerprint motif ((T/S)*X*TG*X*T) in common. The sequence of the fingerprint motif of rubredoxin-oxygen reductase from *Desulfovibrio gigas* deviates from the canonical motif, but this does not affect the FMN binding mode (21). The structure of YLR011wp presents a yet unobserved variation of the flavodoxin loop in FMN-binding proteins. Although the flavodoxin loop of yeast YLR011wp and *B. subtilis* Yhda is longer by two residues, both bind the FMN phosphate in a manner similar to other flavodoxins. A sequence motif search for this YLR011wp loop only revealed its presence in a *Schizosaccharomyces pombe* orthologue (46% sequence identity with YLR011wp) (Fig. 3) and putative reductases from *Streptomyces* and *Bordetella* (having an ~36% sequence identity).

Oligomerization State—Analytical gel-filtration chromatography revealed that YLR011wp exists as a dimer in solution (data not shown). The asymmetric unit of the crystal contains two copies of the molecule related by a 2-fold symmetry axis. The contact area between these two molecules in the asymmetric unit is 2900 Å^2, strongly suggesting that this configuration corresponds to the biologically relevant dimer (22). This obser-

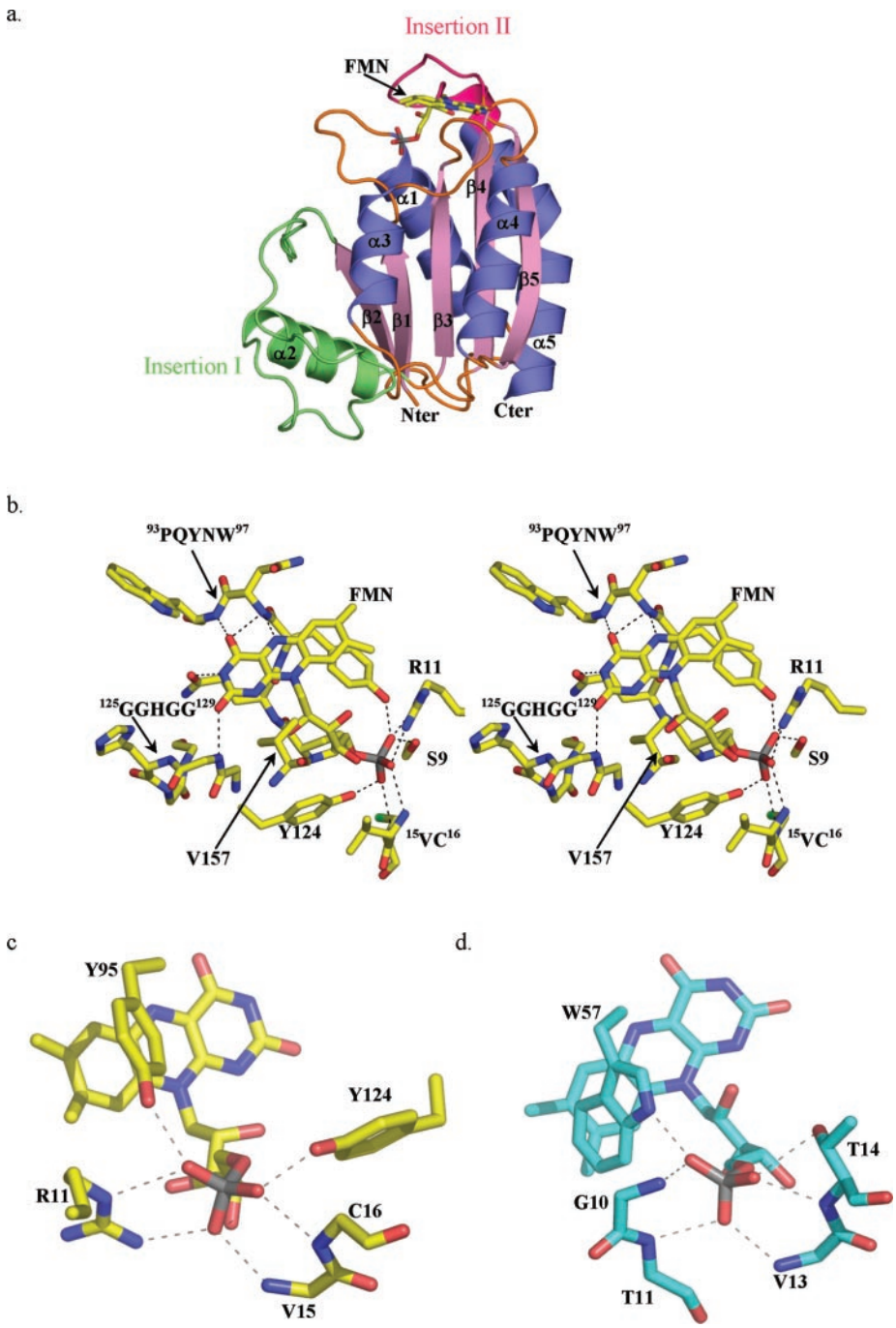

FIG. 1. **YLR011wp structure ribbon representation and FMN binding mode.** *a*, ribbon representation of the YLR011wp monomer. Helices, strands, and loops are colored *blue*, *pink*, and *orange*, respectively. Insertions relative to the canonical flavodoxin fold are colored *green* (*Insertion I*) and *red* (*Insertion II*). Bound FMN is represented by *sticks*. *b*, stereoview of the FMN binding site with the hydrogen bonds indicated by *dashed lines*. The FMN phosphorus and the cysteine sulfur atoms are colored *gray* and *green*, respectively. For clarity, amino acid single letter code is used in every figure. *c* and *d*, stick representation of the FMN phosphate binding mode in YLR011wp (*c*) and in "classical" flavodoxins (*d*) (flavodoxin from *A. nidulans* is considered the classical flavodoxin prototype in our study (5)). For clarity, side chains not involved in hydrogen bonds have been omitted. Hydrogen bonds are depicted by *dashed lines*.

vation is unexpected as most flavodoxin-related proteins, whose structures have been solved, are monomeric (6, 23, 24).

The homodimer has a half-cylinder-like shape with approximate dimensions of 75 × 45 × 40 Å^3 and a large flat solvent-exposed surface. Dimerization occurs mainly via anti-parallel side to side packing of helices α3 and α4 of each monomer (Fig. 2*a*). 21 residues from each monomer are involved in dimer formation. These residues belong to the linkers connecting strand β2 to helix α2 (insertion I: Leu^{45}; Ala^{49}-Tyr^{53}; and Ile$_{60}$) and strand β3 to helix α3 (Tyr^{95}-Tyr^{99}) but also to helices α3 (Ala^{101}, Ala^{102}, Lys^{104}, Asn^{105}, and Asp^{108}) and α4 (Gln^{135}, Glu^{138}, Val^{139}, Gly^{142}, and Leu^{143}). This interface is mainly formed by the packing of hydrophobic residues supplemented by fourteen hydrogen bonds (Table III).

Most of these residues are either absent or not conserved in the monomeric bacterial flavodoxin sequences. However, some other FMN-binding proteins do exist as homodimers. This is the case for *Vibrio harveyi* flavin reductase P (25), *Escherichia coli* nitroreductase NfsA (33), *D. gigas* rubredoxin-oxygen reductase (21), *B. subtilis* Yhda (Protein Data Bank code 1NNI), and probably also for the *E. coli* Trp repressor-binding protein WrbA (26) and *S. cerevisiae* Ycp4 (27), whose structures are still unknown. A comparison of these dimer structures revealed that *E. coli* NfsA and *V. harveyi* flavin reductase P, which share a 52% sequence identity, can be superimposed with an r.m.s.d. as low as 1 Å. As expected from the lack of significant structural resemblance between NfsA (or flavin reductase P) and YLR011wp monomers, the NfsA (or flavin reductase P) and YLR011wp homodimers do not match at all. For the *D. gigas* rubredoxin-oxygen reductase enzyme homodimer, no significant structural alignment can be found with other homodimeric FMN-binding proteins. Among these proteins, the bacterial Yhda is the only one to adopt the same quaternary structure as YLR011wp (r.m.s.d. of 1.5 Å for 260 Cα positions)

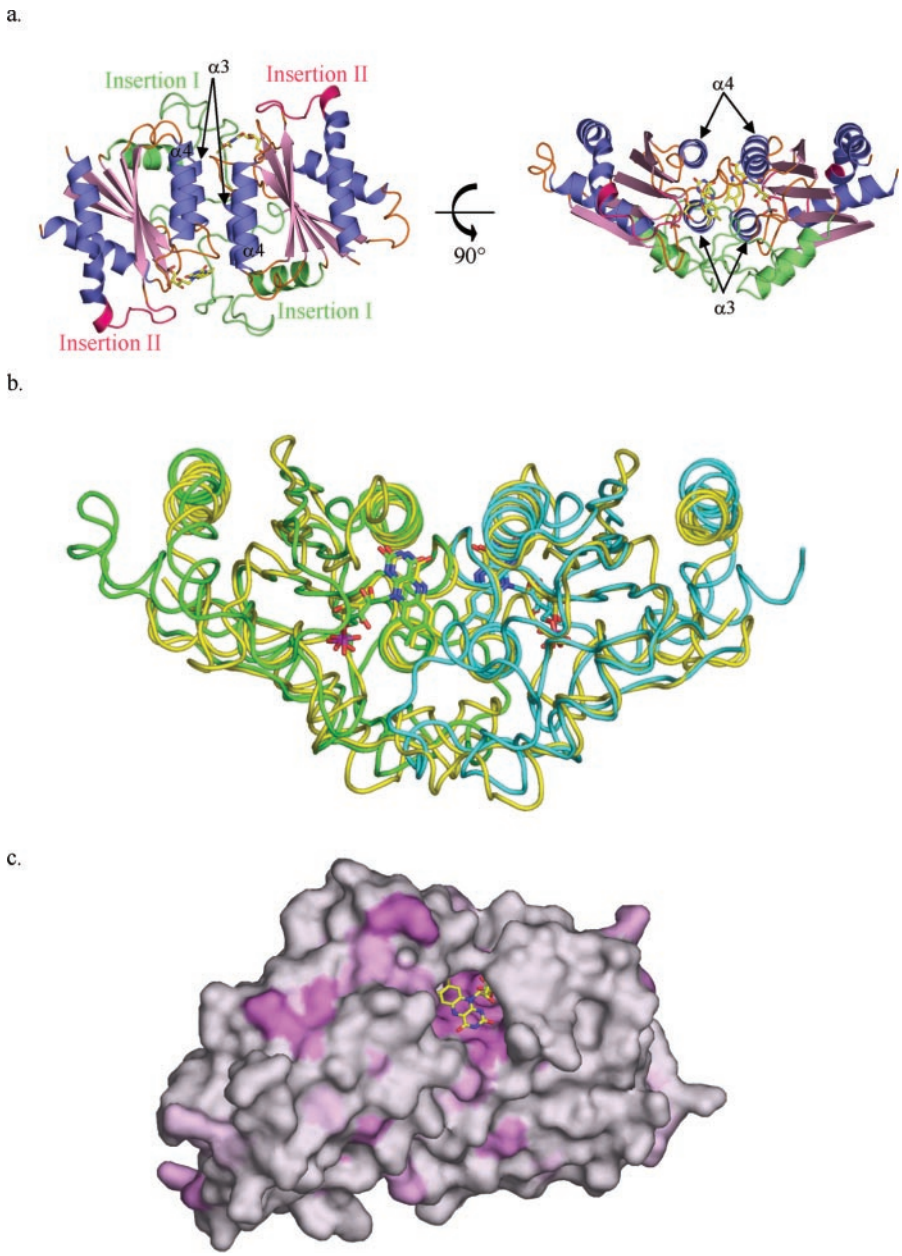

FIG. 2. **The YLR011wp homodimer.** *a*, ribbon representation of the YLR011wp homodimer. The FMN molecules are shown in *sticks*. The dimer in the *right panel* is rotated by 90° along the *x* axis compared with that in the *left panel*. Color coding in this figure is the same as in Fig. 1*a*. *b*, superimposition of the *B. subtilis* Ydha (*yellow*) and the YLR011wp (monomers A and B are in *green* and *blue*, respectively) homodimers. Bound FMNs are shown as *sticks*. *c*, conservation of the residues among the azoreductase enzymes mentioned in Fig. 3. Coloring is from *purple* (highly conserved) to *gray* (low conservation).

TABLE II
Comparison of the polar contacts involved in FMN binding

YLR011wp			Classical flavodoxins[a]		
Protein	FMN	Distance	Protein	FMN	Distance
		Å			Å
Ser^{9} $O_{\gamma[\rho]}$	O_2P	2.4	Thr^{9} $O_{\gamma[\rho]}$	O_1P	2.6
Arg^{11} $N_{\epsilon[\rho]}$	O_2P	3.2	Gln^{10} N	O_2P	2.8
Arg^{11} $N_{\eta[\rho]1}$	O_3P	3	Thr^{11} N	O_3P	3
			Thr^{11} $O_{\gamma1}$	O_3P	2.6
			Gly^{12} N	O_3P	3
Val^{15} N	O_3P	3	Val^{13} N	O_3P	2.8
Cys^{16} N	O_1P	3.1	Thr^{14} N	O_1P	2.8
Tyr^{95} $O_{\eta[\rho]}$	O_2P	2.7	Trp^{57} $N_{\epsilon1}$	O_2P	2.8
Tyr^{124} $O_{\eta[\rho]}$	O_1P	2.5	Thr^{14} $O_{\gamma1}$	O_1P	2.8
Gln^{94} $O_{\epsilon1}$	N_3	3	Asn^{97} O	N_3	2.9
Asn^{96} N	N_5	2.8	Asn^{58} N	N_5	3.4
Asn^{96} N	O_4	3	Val^{59} N	O_4	3.2
Trp^{97} N	O_4	3.2	Gly^{60} N	O_4	2.7
Gly^{126} N	O_2	3	Asp^{90} N	O_2	3.2
			Thr^{56} O	O_2*	2.6
			Asp^{146} $O_{\delta2}$	O_3*	2.7

[a] Classical flavodoxins are those that possess the flavodoxin key fingerprint motif (T/S)*X*TG*X*T. Adapted from Drennan *et al.* (5). Water-mediated hydrogen bonds were not considered.

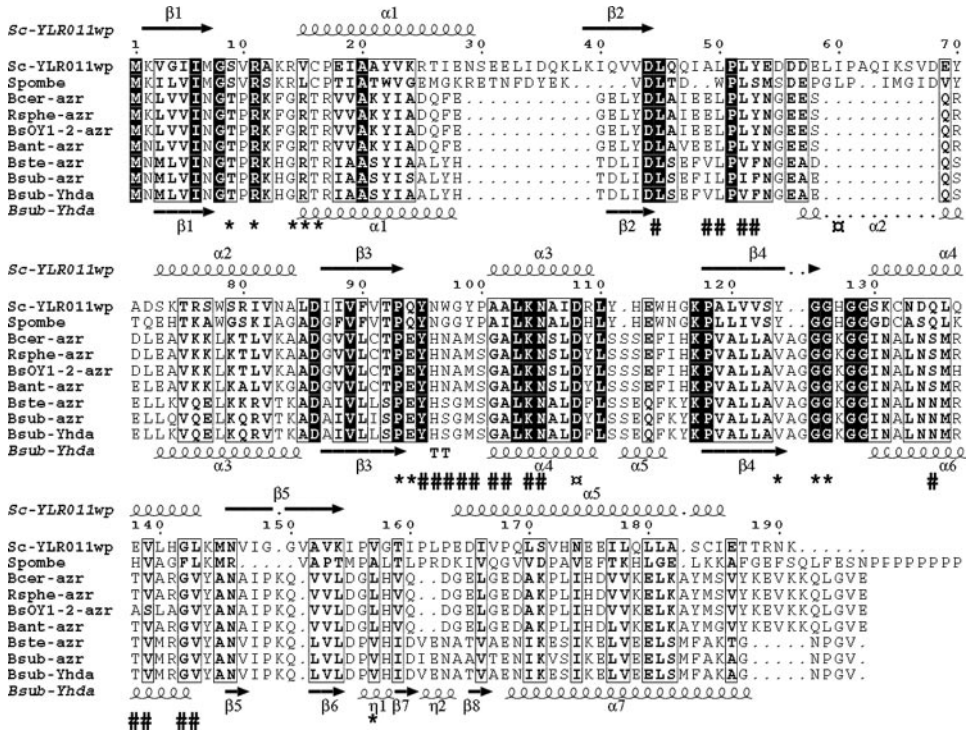

FIG. 3. **Structure-based sequence alignment of YLR011wp orthologues and members of the azoreductase family.** Strictly conserved residues are in *white* on a *black* background. Partially conserved amino acids are *boxed*. YLR011wp positions involved in FMN binding, homodimer formation or both are indicated under the sequence by the following symbols: *; #; and ¤.

TABLE III
Polar and charged interactions involved in dimerization

1st molecule	2nd molecule	Distance
		Å
Ala^{50} O	Tyr^{53} $O_{\eta[\rho]}$	2.4
Tyr^{53} $O_{\eta[\rho]}$	Ala^{50} O	2.3
Tyr^{95} O	Lys^{104} $N_{\zeta[\rho]}$	2.9
Asn^{96} $N_{\delta 2}$	Asp^{108} $O_{\delta 2}$	2.7
Tyr^{99} O	Lys^{104} $N_{\zeta[\rho]}$	2.7
Tyr^{99} $O_{\eta[\rho]}$	Gln^{135} $O_{\epsilon 1}$	2.8
Lys^{104} $N_{\zeta[\rho]}$	Tyr^{95} O	2.8
Lys^{104} $N_{\zeta[\rho]}$	Tyr^{99} O	2.8
Asp^{108} $O_{\delta 2}$	Asn^{96} $N_{\delta 2}$	2.9
Gln^{135} O	Gln^{135} $N_{\epsilon 2}$	2.9
Gln^{135} $O_{\epsilon 1}$	Tyr^{99} $O_{\eta[\rho]}$	2.7
Gln^{135} $N_{\epsilon 2}$	Gln^{138} $O_{\epsilon 1}$	2.9
Gln^{135} $N_{\epsilon 2}$	Gln^{135} O	2.9
Glu^{138} $O_{\epsilon 1}$	Gln^{135} $N_{\epsilon 2}$	2.8

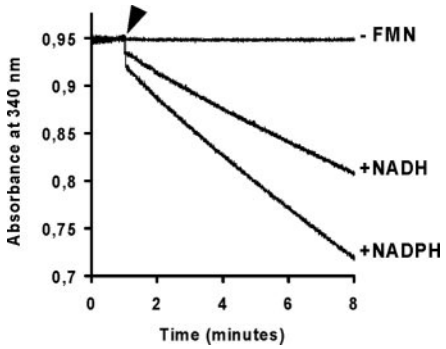

FIG. 4. **YLR011wp NAD(P)H-FMN reductase activity.** YLR011wp (0.24 μM) was preincubated at 30 °C for 1 min in a mixture containing 150 μM NADH or NADPH. Reaction started with the addition of 100 μM FMN (*arrow*), and oxidization of NAD(P)H was followed and recorded at 340 nm *versus* a control cuvette lacking NAD(P)H (ϵ_M NAD(P)H = 6.22 mM^{-1} cm^{-1}).

(aligned dimer structures are represented in Fig. 2*b*). This is supported by a high degree of sequence conservation for most of the residues involved in homodimer formation (Fig. 3). Hence, all of the Yhda homologous proteins described in *Bacillus* subspecies should adopt the same dimer architecture as Yhda and *S. cerevisiae* YLR011wp.

YLR011wp Exhibits Various NAD(P)H-dependent Reductase Activities—Sequence analysis of YLR011wp, whose function is not annotated, assigned this protein to the NADPH-dependent FMN reductase family. The present crystal structure of YLR011wp with bound FMN indeed confirms that it belongs to the flavodoxin family. To our view, YLR011wp forms an interesting test case for deriving biochemical function from the three-dimensional structure.

We first have assayed the enzyme for NAD(P)H-dependent FMN reductase activity by following NAD(P)H oxidation at 340 nm. YLR011wp was able to oxidize NADH and NADPH with a slight preference for the latter. The reaction was strictly dependent on exogenously added FMN (Fig. 4). The specific activity of 0.9 μmol of NADPH oxidized/min/mg protein was measured, a value coherent with FMN reductase-specific activities described for *Salmonella typhimurium* nitroreductase (28) and *E. coli* NfsA and NfsB nitroreductases (29). In many enzymes with NAD(P)H-dependent activity, the FMN reduction step is a prerequisite to additional reductive reaction in which $FMNH_2$ acts as an electron donor (Fig. 5*a*). Therefore, if YLR011wp has a natural acceptor for electron transfer via FMN, the FMN reductase activity detected reflects either the reduction of free oxidized FMN via enzyme-bound FMN (Fig. 5*b*) or the rapid exchange reaction between the reduced and oxidized forms of FMN at the protein FMN binding site (Fig. 5*c*). This latter exchange reaction might not occur when a suitable downstream electron acceptor is present.

We have screened several compounds as electron acceptor candidates for NAD(P)H- and FMN-dependent reduction. We first investigated the YLR011wp capacity to reduce azo dyes *in vitro*. This assumption was based on the close structural resemblance between YLR011wp and *B. subtilis* Yhda that has a 52.8% amino

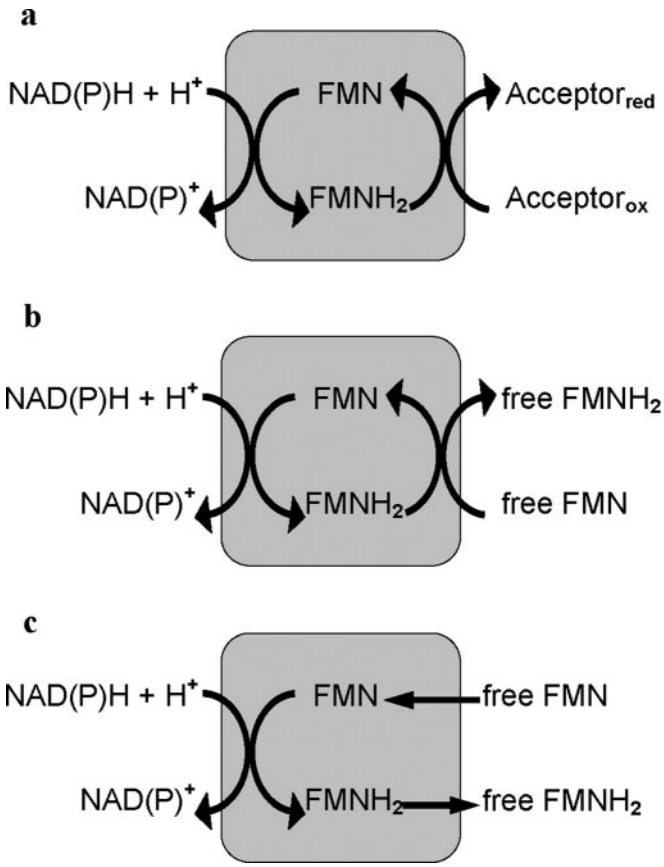

FIG. 5. **General reaction schemes involving NAD(P)H and FMN.** *a*, reaction catalyzed by NAD(P)H- and FMN-dependent oxidoreductases. *b* and *c*, two alternative reactions leading to NAD(P)H-dependent FMN reductase activity: 1) reduction of free FMN via enzyme-bound $FMNH_2$ (*b*) or 2) exchange reaction between reduced and oxidized forms of FMN at FMN binding site (*c*).

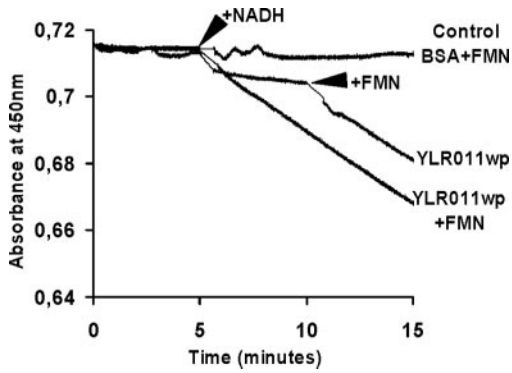

FIG. 6. **YLR011wp azoreductase activity on Ethyl Red is FMN-dependent.** Readings were made *versus* a control cuvette containing a reaction mixture without Ethyl Red. The absorption decrease at 450 nm is shown as function of time (ϵ_M Ethyl Red = 21.56 mM^{-1} cm^{-1}). Protein 2.4 ± 20 μM FMN was incubated for 5 min with Ethyl Red (35 μM). Reaction started with the addition of 100 μM NADH (*left arrowhead*). After 10 min, the reaction mixture was supplemented with 20 μM FMN (*right arrowhead*). *BSA*, bovine serum albumin.

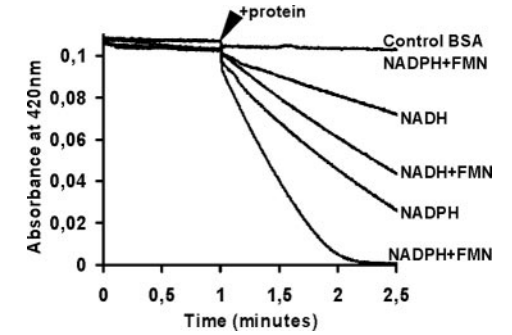

FIG. 7. **YLR011wp ferricyanide reductase activity.** Decrease in absorbance was followed at 420 nm (ϵ_M ferricyanide = 1 mM^{-1} cm^{-1}). Reaction mixture containing 150 μM NAD(P)H ± 20 μM FMN as indicated and 100 μM ferricyanide was incubated at 30 °C for 1 min prior to the addition of protein (YLR011wp or bovine serum albumin (*BSA*) as a control protein, 9 nM each, final concentration).

acid sequence identity with the azoreductase from *Bacillus* sp. OY1–2 (11). These proteins also share a similar FMN binding mode that is different from that of classical flavodoxins. In both proteins, the FMN binding site presents the best-conserved surface patch (Figs. 2*c* and 3). Furthermore, *B. subtilis* Yhda and YLR011wp form identical homodimers (Fig. 2*b*) clearly distinct from quaternary structure arrangements observed for all of the other flavodoxins. Azoreductase assays were performed with a set of four commercially available azo dyes as putative substrate. No activity could be detected with Methyl Red, Orange II, or Reactive Black 5. Clear azoreductase activity could only be demonstrated with Ethyl Red. The decrease in absorbance at 450 nm was dependent on the simultaneous presence of YLR011wp and NADH in the reaction mixture (data not shown). This activity was not dependent on the nature of the electron donor, because both NADH and NADPH gave similar results (data not shown). Ethyl Red reductase activity was almost zero in the absence of exogenously added FMN but could be totally restored by the addition of FMN during the assay (Fig. 6). These data strongly suggest that FMN is necessary for YLR011wp azoreductase activity and that the electron transfer from NAD(P)H to Ethyl Red occurs via FMN. The YLR011wp azoreductase-specific activity measured from our experiments (2–3 nmol of Ethyl Red reduced/min/mg) is several orders of magnitude below the specific activities described for bacterial azoreductases (from a few tens of nmol of azo dye reduced/min/mg up to mmol/min/mg depending on enzyme and substrate) (11, 30–32). Therefore, Ethyl Red, although reduced specifically by YLR011wp, probably does not represent the physiological substrate for YLR011wp.

E. coli NfsA and NfsB nitroreductases are two other examples of enzymes exhibiting weak azo-dependent and standard NAD(P)H-dependent FMN reductase activities but strong ferricyanide reductase activity (29). Therefore, we have tested YLR011wp for ferricyanide and nitroreductase activities. As illustrated in Fig. 7, ferricyanide reductase activity was unambiguously detected and, in our assay, NADPH was a more efficient donor than NADH. The presence of 20 μM FMN during the assay increased sensibly the rate of the reaction. Therefore, as already mentioned for YLR011wp azoreductase activity, the electron transfer from NAD(P)H to the ferricyanide acceptor occurs via FMN. Ferricyanide proved to be an excellent acceptor as a specific activity of 625 μmol of ferricyanide reduced/min/mg was calculated from the assay with NADPH as a donor and 20 μM FMN (Fig. 7). This level of ferricyanide reductase activity is comparable with the levels described for NfsA and NfsB nitroreductases (29). However, only very weak nitroreductase activity could be detected with YLR011wp using nitrofurazone as an electron acceptor compared with that of NfsA and NfsB (10–20 nmol/min/mg for YLR011wp and 73 and 13 μmol/min/mg for NfsA and NfsB, respectively).

From these enzymatic data, it is still difficult to conclude on the precise biochemical function of YLR011wp. Although several specific reductase activities have been characterized using NAD(P)H as an electron donor and FMN as a cofactor, only ferricyanide reductase assays gave high specific activity. We propose that ferric iron, present in the ferricyanide complex, may be the natural substrate for the reduction catalyzed by this protein. Ferric iron reduction is the central reaction in

cellular iron metabolism. Microbial cells have developed different systems for iron uptake (33). In budding yeast, Arn1–4 permeases import extracellular ferric chelates and iron siderophores, whereas Frt1 plasma membrane transporter is specific for free ferric iron. In both cases, the cell indeed has to convert cytosolic ferric iron (free or chelated) into ferrous iron before its incorporation into heme- and nonheme iron-containing proteins. The cytosolic protein responsible for ferric iron reduction is still unknown despite previous biochemical studies (34). From our data, YLR011wp is a good candidate for cytosolic ferric iron reductase activity in yeast and further experiments are needed to reinforce this hypothesis.

In conclusion, we clearly show that YLR011wp is a flavodoxin that binds an FMN cofactor despite the absence of the flavodoxin key fingerprint motif ((T/S)*X*TG*X*T) usually involved in FMN phosphate binding. The protein exists as a homodimer in the crystal as well as in solution. The biochemical studies aimed to identify YLR011wp *in vivo* activity showed that the protein bears several reductase activities that are NAD(P)H-dependent and involve FMN as a cofactor. Ferricyanide was by far the best substrate for reduction, strongly suggesting that this protein could be involved in ferric iron assimilation.

REFERENCES

1. Simondsen, R. P., and Tollin, G. (1980) *Mol. Cell Biochem.* **33,** 13–24
2. Blaschkowski, H. P., Neuer, G., Ludwig-Festl, M., and Knappe, J. (1982) *Eur. J. Biochem.* **123,** 563–569
3. Bianchi, V., Eliasson, R., Fontecave, M., Mulliez, E., Hoover, D. M., Matthews, R. G., and Reichard, P. (1993) *Biochem. Biophys. Res. Commun.* **197,** 792–797
4. Fukuyama, K., Matsubara, H., and Rogers, L. J. (1992) *J. Mol. Biol.* **225,** 775–789
5. Drennan, C. L., Pattridge, K. A., Weber, C. H., Metzger, A. L., Hoover, D. M., and Ludwig, M. L. (1999) *J. Mol. Biol.* **294,** 711–724
6. Freigang, J., Diederichs, K., Schafer, K. P., Welte, W., and Paul, R. (2002) *Protein Sci.* **11,** 253–261
7. Wang, M., Roberts, D. L., Paschke, R., Shea, T. M., Masters, B. S., and Kim, J. J. (1997) *Proc. Natl. Acad. Sci. U. S. A.* **94,** 8411–8416
8. White, K. A., and Marletta, M. A. (1992) *Biochemistry* **31,** 6627–6631
9. Chikuba, K., Yubisui, T., Shirabe, K., and Takeshita, M. (1994) *Biochem. Biophys. Res. Commun.* **198,** 1170–1176
10. Zhang, L., Ohta, A., Horiuchi, H., Takagi, M., and Imai, R. (2001) *Biochem. Biophys. Res. Commun.* **283,** 531–535
11. Suzuki, Y., Yoda, T., Ruhul, A., and Sugiura, W. (2001) *J. Biol. Chem.* **276,** 9059–9065
12. Roth, M., Carpentier, P., Kaikati, O., Joly, J., Charrault, P., Pirocchi, M., Kahn, R., Fanchon, E., Jacquamet, L., Borel, F., Bertoni, A., Israel-Gouy, P., and Ferrer, J. L. (2002) *Acta Crystallogr. Sect. D Biol. Crystallogr.* **58,** 805–814
13. Otwinowski, Z., and Minor, W. (1997) *Methods Enzymol.* **276,** 307–326
14. Terwilliger, T. C., and Berendzen, J. (1999) *Acta Crystallogr. Sect. D Biol. Crystallogr.* **55,** 849–861
15. Terwilliger, T. C. (1999) *Acta Crystallogr. Sect. D Biol. Crystallogr.* **55,** 1863–1871
16. Roussel, A., and Cambillau, C. (1989) pp. 77–78, Silicon Graphics, Mountain View, CA
17. Murshudov, G. N., Vagin, A. A., and Dodson, E. J. (1997) *Acta Crystallogr. Sect. D Biol. Crystallogr.* **53,** 240–255
18. Laskowski, R. A., MacArthur, M. W., Moss, D. S., and Thornton, J. M. (1993) *J. Appl. Crystallogr.* **26,** 283–291
19. Rao, S. T., Shaffie, F., Yu, C., Satyshur, K. A., Stockman, B. J., Markley, J. L., and Sundarlingam, M. (1992) *Protein Sci.* **1,** 1413–1427
20. Mayhew, S. G., and Ludwig, M. L. (1975) *Flavodoxins and Electron-transferring Flavoproteins*, Academic Press, New York, NY
21. Frazao, C., Silva, G., Gomes, C. M., Matias, P., Coelho, R., Sieker, L., Macedo, S., Liu, M. Y., Oliveira, S., Teixeira, M., Xavier, A. V., Rodrigues-Pousada, C., Carrondo, M. A., and Le Gall, J. (2000) *Nat. Struct. Biol.* **7,** 1041–1045
22. Janin, J., and Rodier, F. (1995) *Proteins* **23,** 580–587
23. Watenpaugh, K. D., Sieker, L. C., and Jensen, L. H. (1973) *Proc. Natl. Acad. Sci. U. S. A.* **70,** 3857–3860
24. Hoover, D. M., and Ludwig, M. L. (1997) *Protein Sci.* **6,** 2525–2537
25. Tanner, J. J., Lei, B., Tu, S. C., and Krause, K. L. (1996) *Biochemistry* **35,** 13531–13539
26. Yang, W., Ni, L., and Somerville, R. L. (1993) *Proc. Natl. Acad. Sci. U. S. A.* **90,** 5796–5800
27. Toda, T., Shimanuki, M., Saka, Y., Yamano, H., Adachi, Y., Shirakawa, M., Kyogoku, Y., and Yanagida, M. (1992) *Mol. Cell. Biol.* **12,** 5474–5484
28. Watanabe, M., Nishino, T., Takio, K., Sofuni, T., and Nohmi, T. (1998) *J. Biol. Chem.* **273,** 23922–23928
29. Zenno, S., Koike, H., Kumar, A. N., Jayaraman, R., Tanokura, M., and Saigo, K. (1996) *J. Bacteriol.* **178,** 4508–4514
30. Chen, H., Wang, R. F., and Cerniglia, C. E. (2004) *Protein Expression Purif.* **34,** 302–310
31. Nakanishi, M., Yatome, C., Ishida, N., and Kitade, Y. (2001) *J. Biol. Chem.* **276,** 46394–46399
32. Moutaouakkil, A., Zeroual, Y., Zohra Dzayri, F., Talbi, M., Lee, K., and Blaghen, M. (2003) *Arch Biochem. Biophys.* **413,** 139–146
33. Schroder, I., Johnson, E., and de Vries, S. (2003) *FEMS Microbiol. Rev.* **27,** 427–447
34. Lesuisse, E., Crichton, R. R., and Labbe, P. (1990) *Biochim. Biophys. Acta* **1038,** 253–259